Obfitości pierwiastków w koronie słonecznej

Elemental Abundances in the Solar Corona

Barbara Sylwester

CBK PAN

References

Active region's composition analysis

Establishing a connection between active region outflows and the solar wind: Abundance measurements with EIS/Hinode;
Davod H. Brooks & Harry P. Warren, ApJ Letters, 727, L13, 2011

Plasma composition in a sigmoidal anemone active region **(young AR)**
D. Baker, D. H. Brooks, P. Demoulin, L. van Driel-Gesztelyi, L. M. Green, K. Steed, and J. Carlyle; 2013, ApJ, 778, 69

FIP bias evolution in a **decaying** active region;
Baker, D. , D. H. Brooks, P. Démoulin, S. L. Yardley, L. van Driel-Gesztelyi, D. M. Long, and L. M. Green, ApJ, 802, 2015

Flares

Elemental Abundances in the Solar Corona as Measured by the X-ray Solar Monitor Onboard Chandrayaan;
S. Narendranath, P. Sreekumar, L. Alha, K. Sankarasubramanian, J. Huovelin, P.S. Athiray
Solar Phys., 289, 2014

RESIK solar X-ray flare element abundances on non-isothermal assumption; B. Sylwester, K.J.H. Phillips, J. Sylwester, A. Kępa, ApJ, 2015, accepted

Solar flare composition and thermodynamics from RESIK X-ray spectra; B. Sylwester, J. Sylwester, K. J. H. Phillips, A. Kępa, and T. Mrozek, 2014, ApJ, 787

Plasma composition in AR
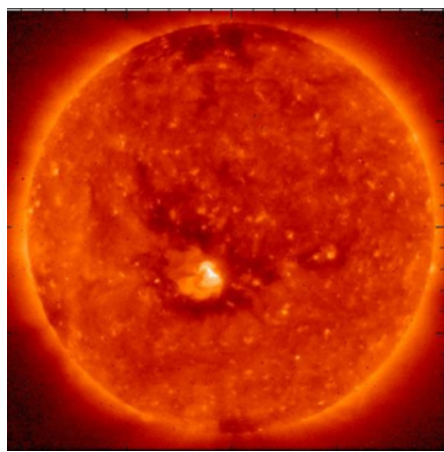
Hinode/EUV Imaging Spectrometer (EIS) → observes in two wavelength bands: 171–212 Å and 245–291 Å, 1" spatial resolution (pixel size), spectral resolution of 22.3 mÅ → detailed spatially resolved abundance map of AR-CH complex based on S X λ=264.223 Å and Si X λ=258.375 Å lines. **Small & young AR inside low-latitude CH; 359"×485" one raster scan on 17 Oct. 2007 at 02:47 UT**

← **Hinode/XRT Al mesh filter full-disc image for 2007 October 17**

1. Coaligned intensity images for all spectral lines
2. Fitted Gaussians to strong lines Fe VIII-XVI and S X λ264.223 and Si X   λ258.375
3. Determine **density** in each pixel (from Fe XIII λ202.044/λ203.826 diagnostic ratio)
4. Calculate contributions functions using CHIANTI **with determined density and photospheric abundances assumed**
5. Calculating **DEM** using Markov Chain Monte Carlo (MCMC) algorithm available with the PINTofALE spectroscopy package and **10 Fe lines from Fe VIII 185.213 Å to Fe XVI 262.984 Å** (FIP Fe=7.87 eV). Once the DEM is computed the S x 264.233 Å line intensities are calculated. (FIP S=10.36 eV)
6. For each of **170 000** pixels in the raster calculated intensities are fit to the observed intensities to determine the best solution → FIP bias
7. Calculate FIP bias: ratio of observed to calculated (predicted) intensity for S X λ264.233 line FIP bias=A_{sa}/A_{ph}

AR & CH complex; morphological grouping of FIP bias structures
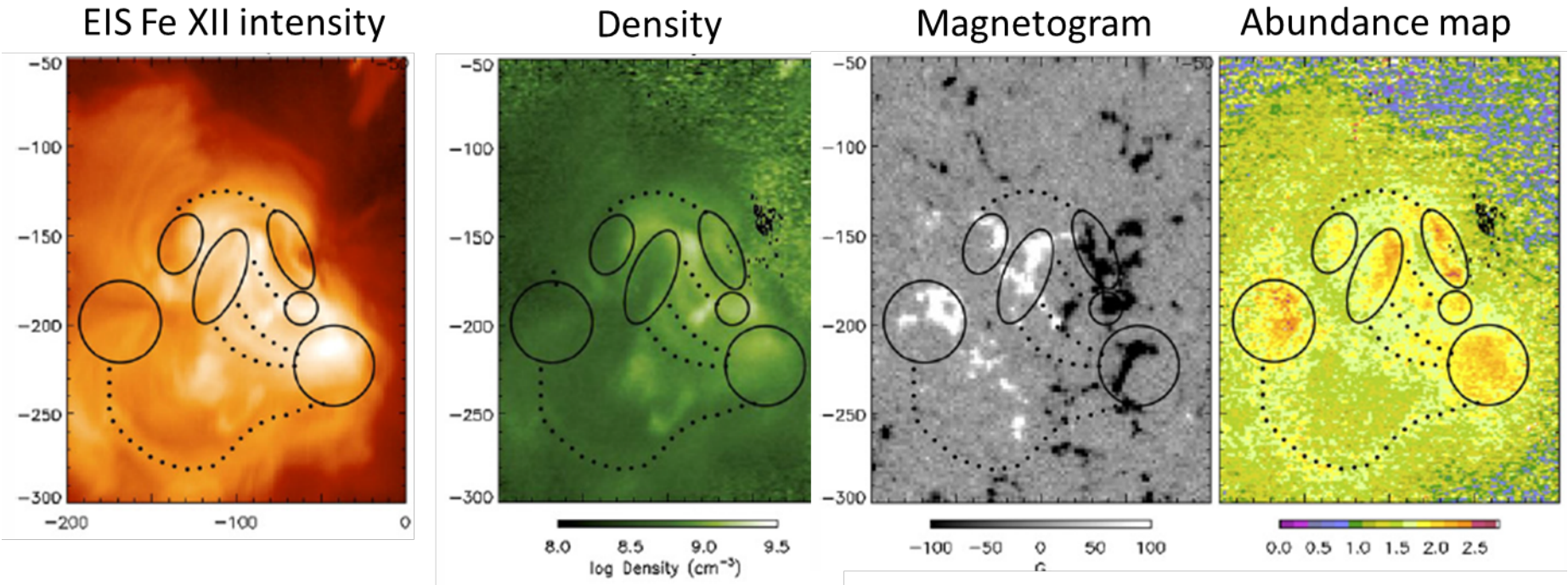
Surrounding CH → photospheric composition (FIP bias=1)

High (2.5-3) FIP bias regions (coronal composition) located in a few patches at loops footpoints close to regions of strong magnetic flux (solid black ellipses) and loop traces of enhanced (2-2.5) FIP bias (dotted black curves).
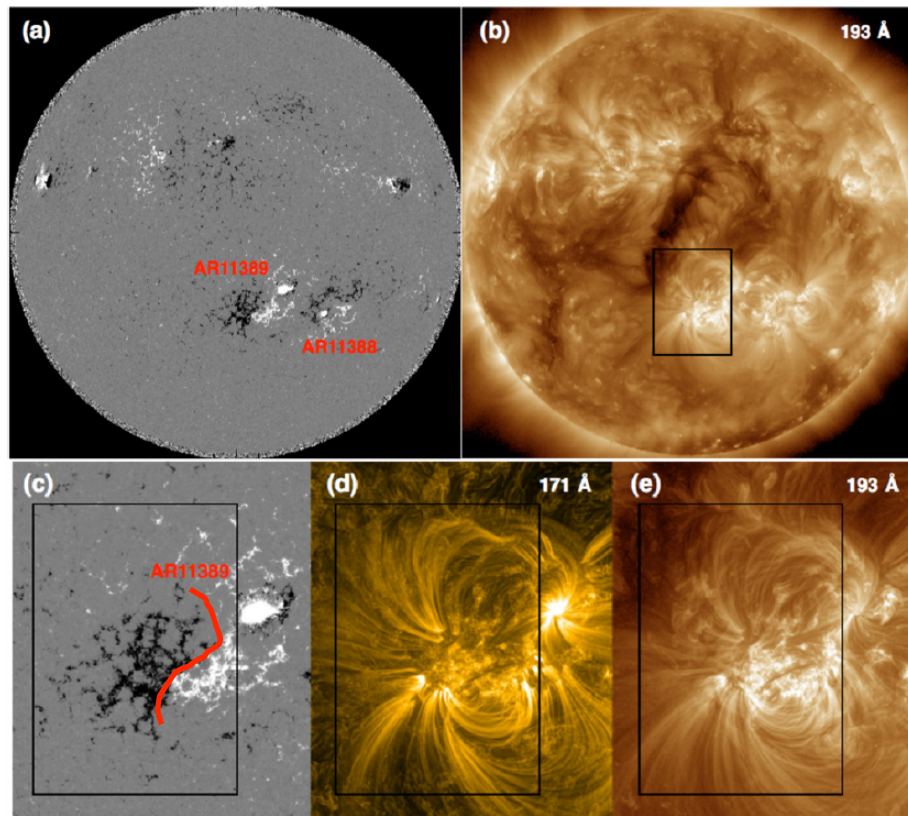
FIP bias in the small relatively young AR is 2-3.

# FIP bias evolution in a **decaying AR**

Top: Images of AR-CH complex on 2012 January 4 at 08:00 UT
(a) Full disk SDO/HMI magnetogram
(b) SDO/AIA 193 Å image (CH seen)
Bottom: Zoomed images (c) SDO/HMI, (d) SDO/AIA 171 Å and (e) 193 Å high-resolution

Observations during 2012 January 4-6
AR 11389 expected to be older than 2 weeks but less than 1 month:
Appeared on 2011 Dec. 28 (*Hinode*)
Seen in STEREO B on 2011 Dec. 20
Raster → FOV: 360"x512"

Hinode/EUV Imaging Spectrometer (EIS)
SDO/Atmospoheric Imaging Assembly (AIA)
SDO/Helioseismic and Magnetic Imager (HMI)

Loops NOT isolated from the background
Based on the composition maps AR has been divided into regions R1-R5 (R3 into subregions). **Polarity inversion line (PIL)** used as the reference for the placement of regions on 6th Jan.

Composition maps overplotted with contours designating major regions and subregions

4 Jan.

R5

PIL

R4

R3

c

d

b

a

R1

R2

(a)

6 Jan.

R5

(b)
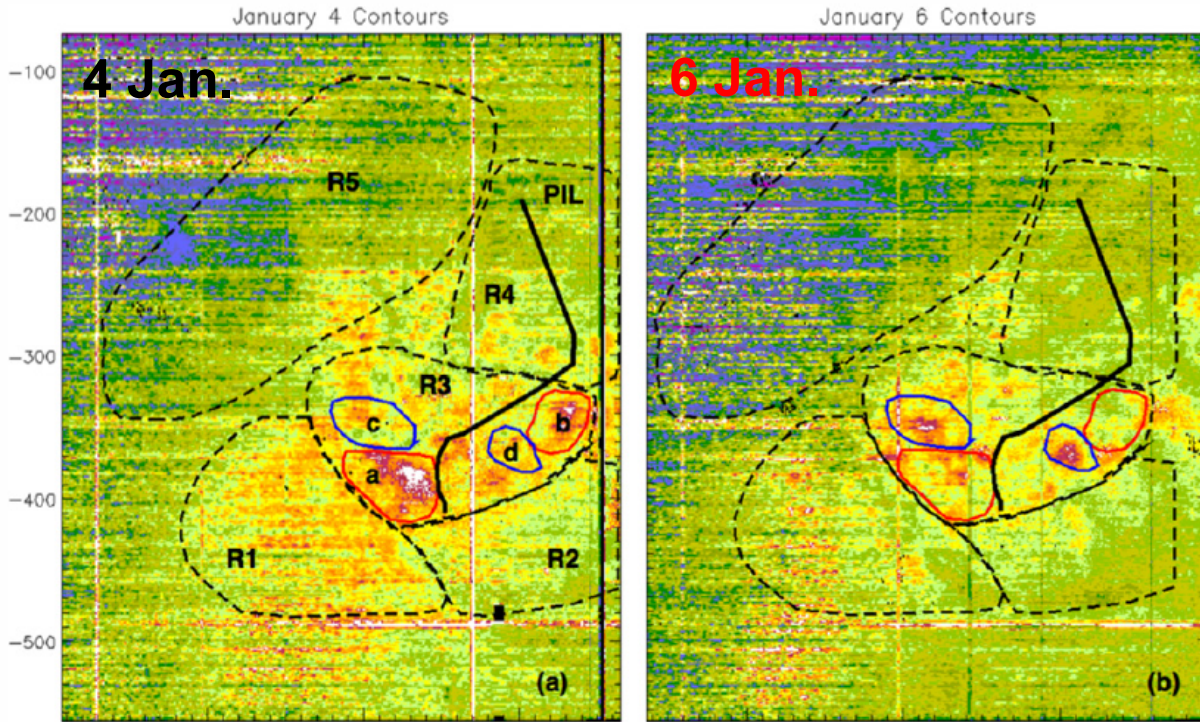
The big change observed in the composition maps **over two days** is the **decrease** in FIP bias in **R1** (within the negative field 8 emerging positive magnetic fragments appeared). Small bipoles emerging reconnected with the pre-existing coronal field. *As a consequence of the reconnection, photospheric plasma contained within these bipoles mixed with high-FIP bias plasma of the coronal loops leading to decrese in FIP bias.*

Changes in FIP bias occur in other localized regions (R2–R4) and along its north – eastern edge (R5), adjacent to the CH.

R3 (**AR core**) divided into 4 subregions indicated more localized changes. Contours **3a–3b (red)** are located at the footpoints of one set of connecting sheared coronal loops and **3c–3d (blue)** are located at the footpoints of different set of less sheared loops.

Probability distribution functions (PDFs) of FIP bias/pixel
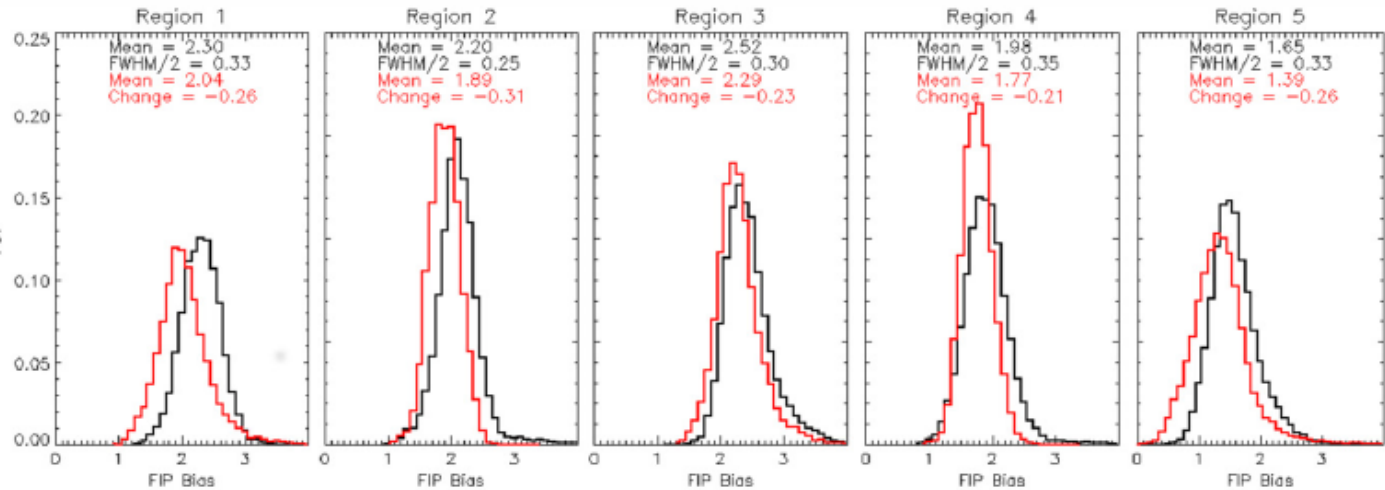
PDFs of FIP bias in regions R1, R2, R4, and R5 show clear shifts **toward photospheric** composition after 2 days.
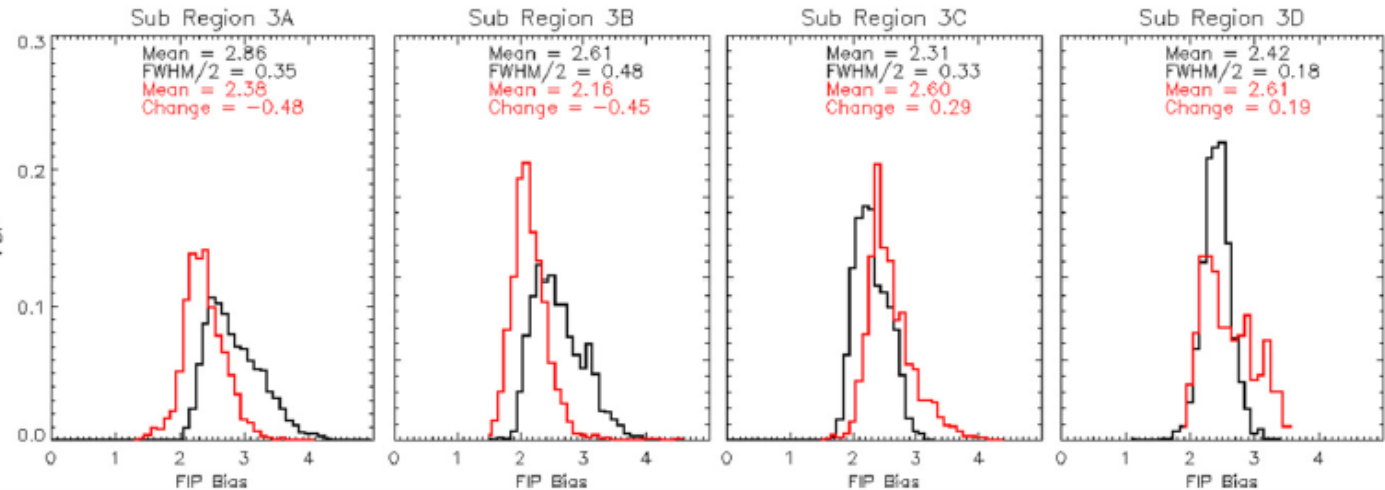
In the case of 3a–3b, FIP bias substantially **decreases** with mean values 0.48 and 0.45 respectively in contrast to footpoints of the coronal loops connecting 3c–3d where FIP bias **increases**.

2012 January 4 at 09:40 UT   **2012 January 6 at 13:40 UT**

Conclusions

Evidence of FIP bias evolution in a **decaying AR** near a CH from 2012 January 4 to 6 using SDO/AIA, SDO/HMI, and Hinode/EIS observations.

Small-scale evolution of the underlying magnetic field **is closely linked** to the evolution of plasma composition observed in the corona.
*For all regions and subregions where **FIP bias decreased**, episodes of **flux emergence/cancellation** and moving magnetic features were identified.*

High-FIP bias is **conserved/amplified** only in localized areas of high magnetic flux density i.e., in the AR core. In all other areas within the AR, FIP bias decreased.

Elemental Abundances in the Solar Corona as Measured by the X-ray Solar Monitor (XSM) Onboard Chandrayaan-1

Shyama Narendranath, P. Sreekumar, L. Alha, K. Sankarasubramanian, J. Huovelin, P.S. Athiray
Solar Phys., 289, 2014

Indian Space Research Organisation & Indian Institute of Astrophysics, Bangalore, India
Division of Geophysics and Astronomy, University of Helsinki, Finland

XSM measured the 1.8 – 20 keV solar X-ray spectrum with temporal resolution 16 sec. during its 9 months (28 November 2008 to 29 August 2009) of operation in lunar orbit (20 min. of data every orbit). XSM is a non-imaging, wide-field spectrometer and covers the full solar disk. **XSM was developed at the University of Helsinki in Finland** and consists of a Si-PIN detector with a Peltier cooler. XSM measured several X-ray flare spectra at moderately good resolution (200 eV at 5.9 keV).

X-ray Solar Monitor (XSM) on first Indian lunar mission Chandrayaan-1

XSM was calibrated pre-launch at the University of Helsinki and additionally at the RESIK X-ray beam facility at RAL, UK. A built-in calibration source, a Fe-55 radioisotope with Ti foil, provided four lines (at 4.5 keV, 4.9 keV, 5.9 keV, and 6.4 keV) in orbit for calibration.
At the beginning of every observation (sunlit-side in the lunar orbit) 400 seconds of calibration data are collected, after which the shutter opens for solar observation.

Coronal abundances of the **low-FIP elements Fe, Ca, Si, (7.87 eV, 6.11 eV, 8.15 eV)** and **S (intermediate FIP element,10.36 eV**) and their temporal evolution during a C2.8 flare on 5 July 2009 (the brightest observed) have been analysed.

Sulfur abundances determined for decay phases of 20 *GOES*-class flares (A, B, and C).

Representative spectral fits to flare spectra

5 July 2009

07:12:17 - 07:12:49 UT

8 July 2009

07:13:53 - 07:14:25 UT

4 July 2009
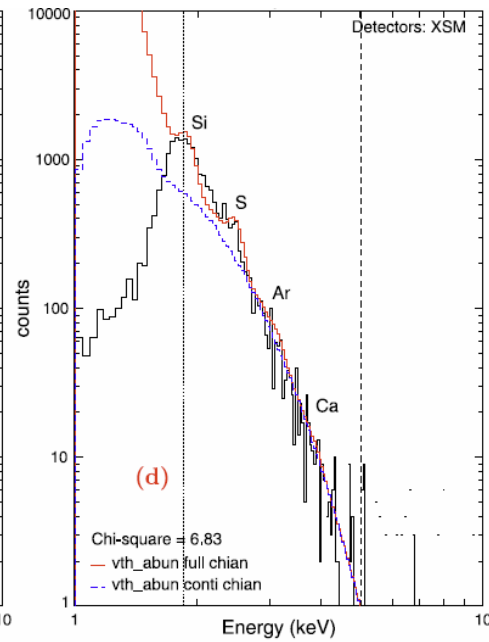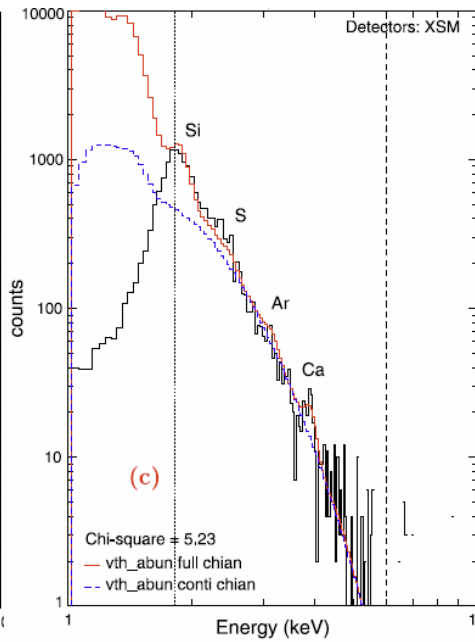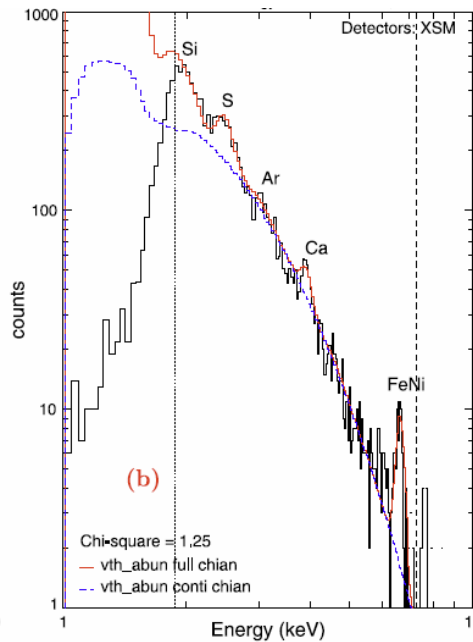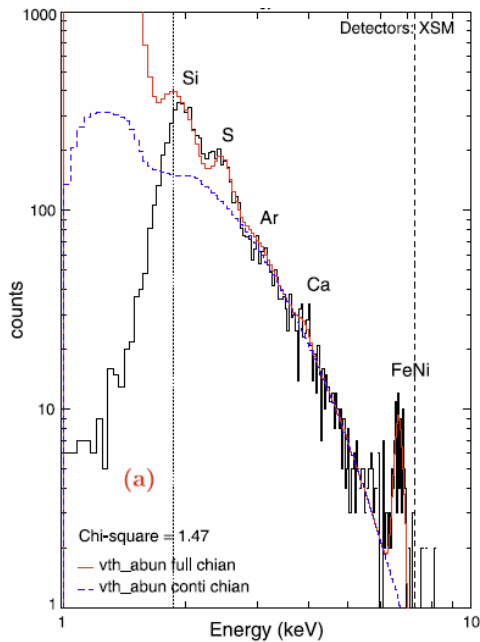
03:06:03 - 03:13:15 UT

22:28:31 - 22:43:43 UT

The vertical lines indicate the range of energies fitted. The red line is the best-fit model and the dotted blue line shows the thermal bremsstrahlung continuum (1.8 – 8 keV).

Spectra from weaker flares where the Fe line complex is not visible.

Analysis

The spectral analysis was carried out with the OSPEX (Object Spectral Executive) package.

The temperature and emission measure are determined from the soft X-ray continuum in the 1.8 – 8 keV range.

The abundances are obtained from the intensities of resolved emission-line complexes.

The spectra were fitted with a thermal model (single temperature) calculated from CHIANTI which consists of a continuum and emission lines. Correction factors (F) over the coronal abundance assumed in the model $A(E)_{FL}$ (Feldman, 1992) are free parameters, which were varied during the fit.

$$A(E) = log(F) + A(E)_{FL}$$

Characteristics obtained for C2.8 flare
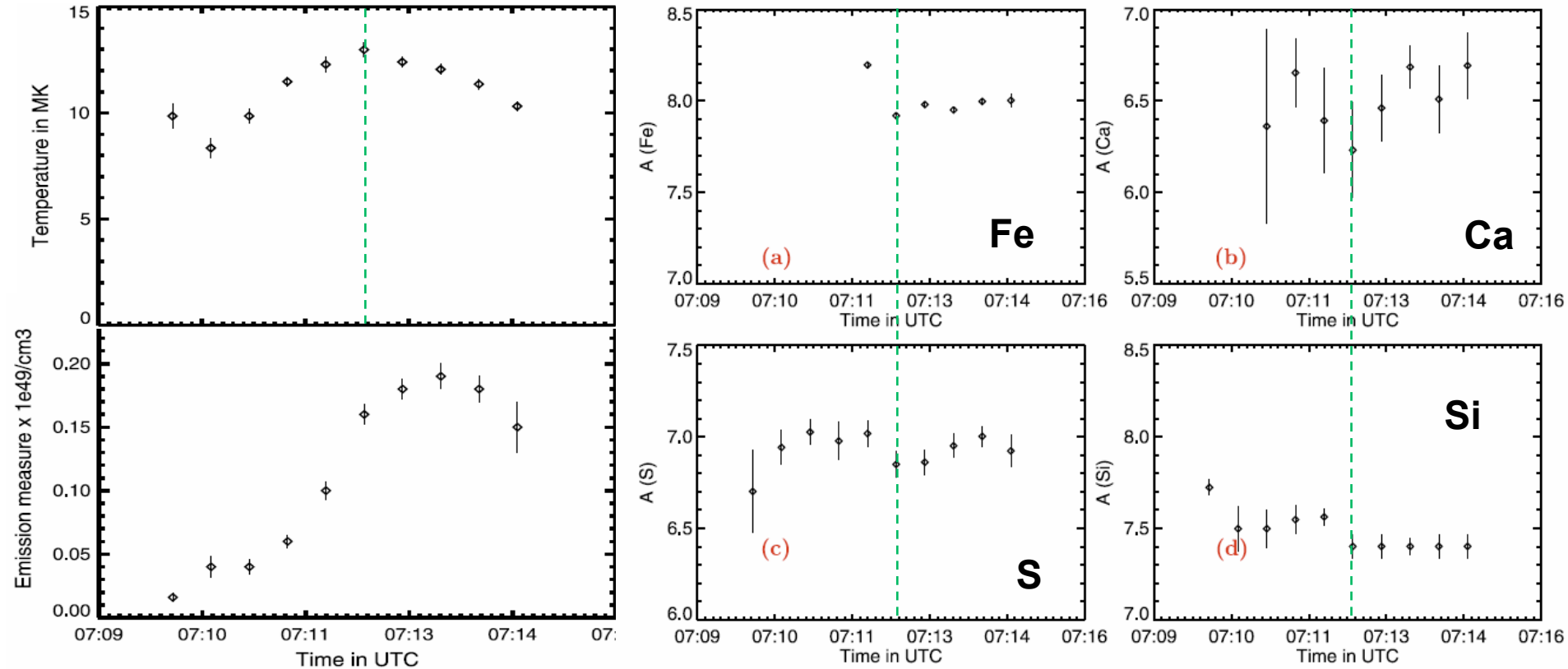
The temperature and emission measure are determined from the soft X-ray continuum in the 1.8 – 8 keV range.

$$A(E) = log(F) + A(E)_{FL}$$

Correction factors (**F**) over the coronal abundance assumed in the model $A(E)_{FL}$ (Feldman, 1992) are free parameters, which were varied during the fit.

A(S) from all of flares analysed
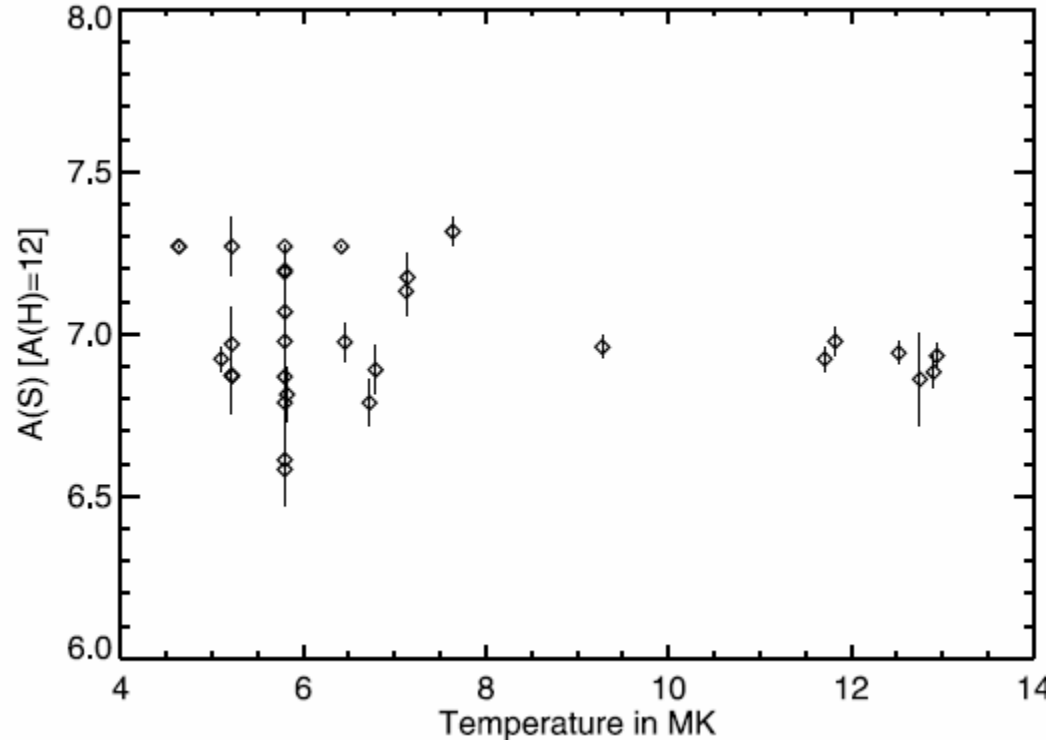
The derived abundances of S against the plasma temperature.
These estimates are spread over a wide range of temperatures, suggesting
that abundances are slightly lower for higher temperatures (????????).
….. …the data are not sufficient to establish this conclusively

Analysis of 33 flare's spectra observed with RESIK

Solar flare composition and thermodynamics from RESIK X-ray spectra; B. Sylwester, J. Sylwester, K. J. H. Phillips, A. Kępa, and T. Mrozek, ApJ, 787, 2014

RESIK solar X-ray flare element abundances on non-isothermal assumption; B. Sylwester, K.J.H. Phillips, J. Sylwester, A. Kępa, ApJ, 2015, accepted

Analysed flares: located on the disc and limb, short and long duration, different X-ray classes (mainly C & M)
1 of B (B9.9)
26 of C
5 of M
1 of X (X1.5, rise & decay only)
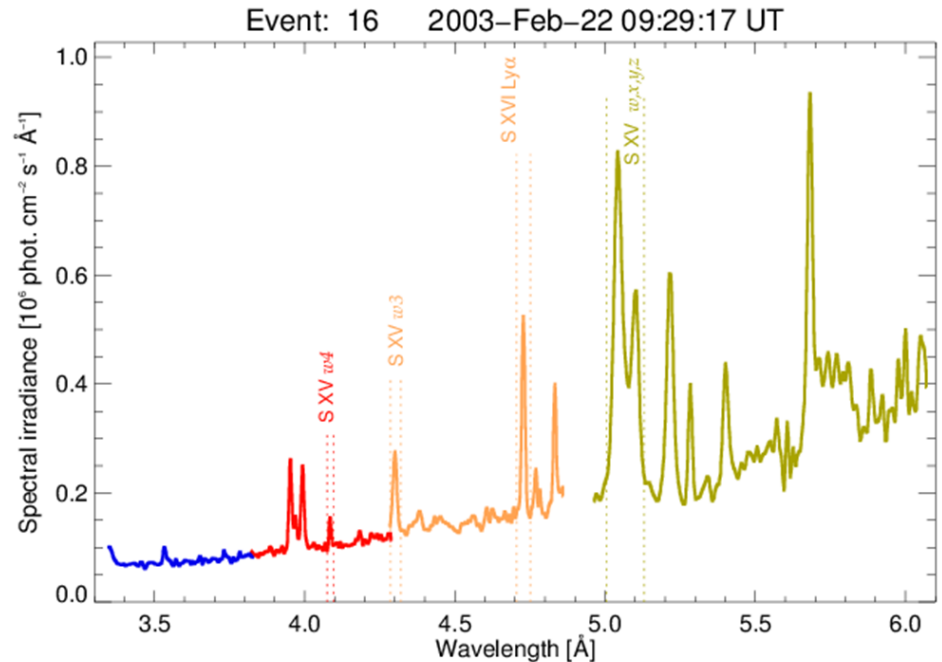
RESIK spectrum analysis

2003–Jan–09 00:14:00   2003–Jan–09 02:08:23

exposure = 43.3 min

(Spectrum plot: 10^6 [Phot. cm^{-2} s^{-1} Å^{-1}] vs Wavelength [Å], labeled emission features: Si XIII 3p, S XV w,x,y,z, Si XIV 3p, Si XIII 4p, Si XII sat, S XVI 2p, Si XIV 5p, Si XIII 5p, Si XII sat, Ar XVII w,x,y,z, S XIV sat, S XV 4p, S XV 3p, K XVIII w,x,y,z, Ar XVIII 2p)
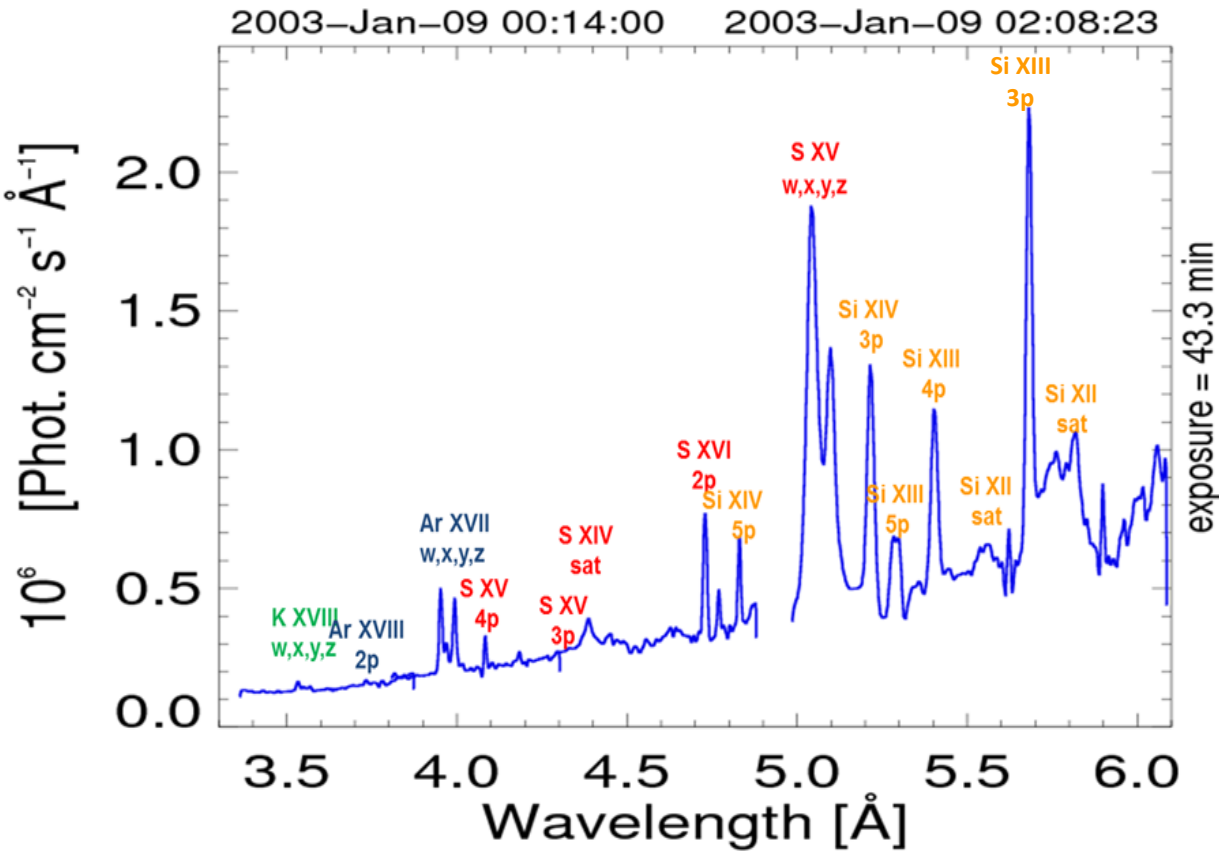
- 18 spectral intervals
- 4 elements (K, Ar, S, Si)
- **21 values of abundance for each element (0.1-16 times coronal value)**
- Abundance corresponding to min. X^2 is the optimum one.

$$F_i = A_i \int_{T=0}^{\infty} f_i(T)\varphi(T)\,dT$$

No.	Wavelength range (Å)	RESIK Channel	Emission features included
1	3.40 - 3.50	1	continuum
2	3.50 - 3.60	1	K XVIII triplet + sats.
3	3.60 - 3.80	1	continuum
4	3.915 - 4.025	2	Ar XVII triplet + sats.
5	4.11 - 4.17	2	continuum
6	4.17 - 4.21	2	S XV $1s^2 - 1s4p$ sats.
7	4.21 - 4.25	2	continuum
8	4.36 - 4.42	3	S XV d3 sats.
9	4.42 - 4.68	3	continuum
10	4.70 - 4.75	3	S XVI Lyα
11	4.75 - 4.80	3	S XV sats to S XVI Lyα
12	5.00 - 5.15	4	S XV triplet + sats.
13	5.25 - 5.32	4	Si XIII $1s^2 - 1s5p$
14	5.37 - 5.48	4	Si XIII $1s^2 - 1s4p + 5p$ sat.
15	5.48 - 5.62	4	Si XII 4p sats.
16	5.645 - 5.71	4	Si XIII $1s^2 - 1s3p$
17	5.77 - 5.86	4	Si XII 3p sat.
18	5.92 - 5.97	4	continuum

Results for individual flares

6.02±0.15

6.31±0.07

7.00±0.02

7.49±0.04

5.70±0.16

6.44±0.05

6.88±0.04

7.50±0.10
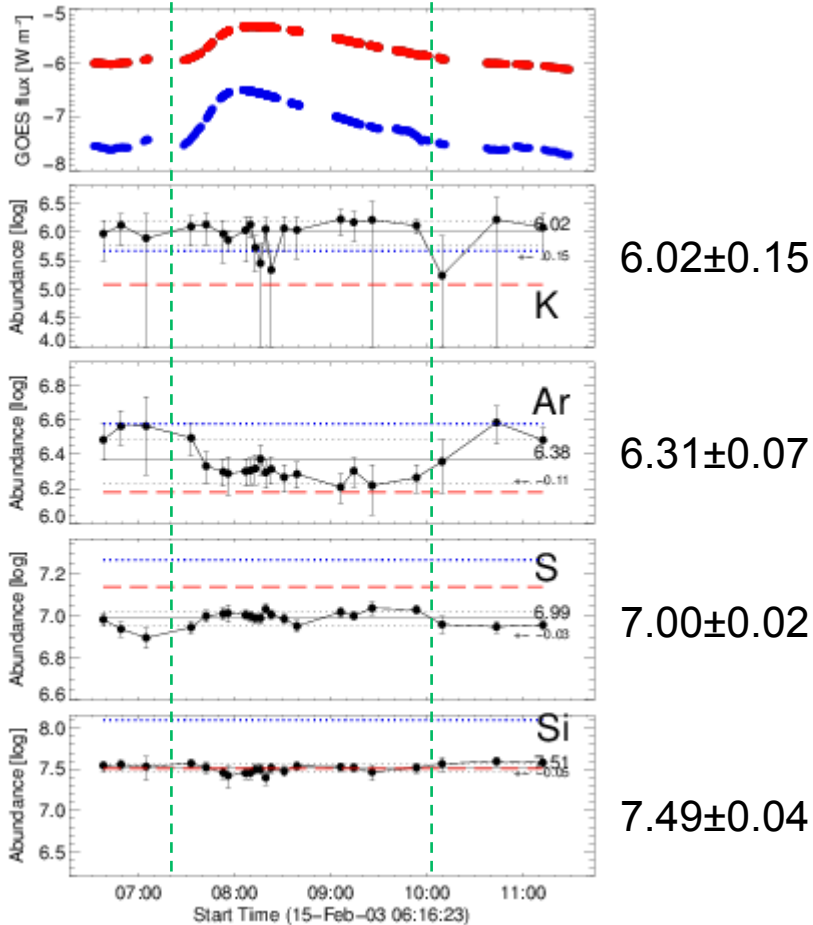
15 Feb. 2003 ~08:10 UT C 4.5
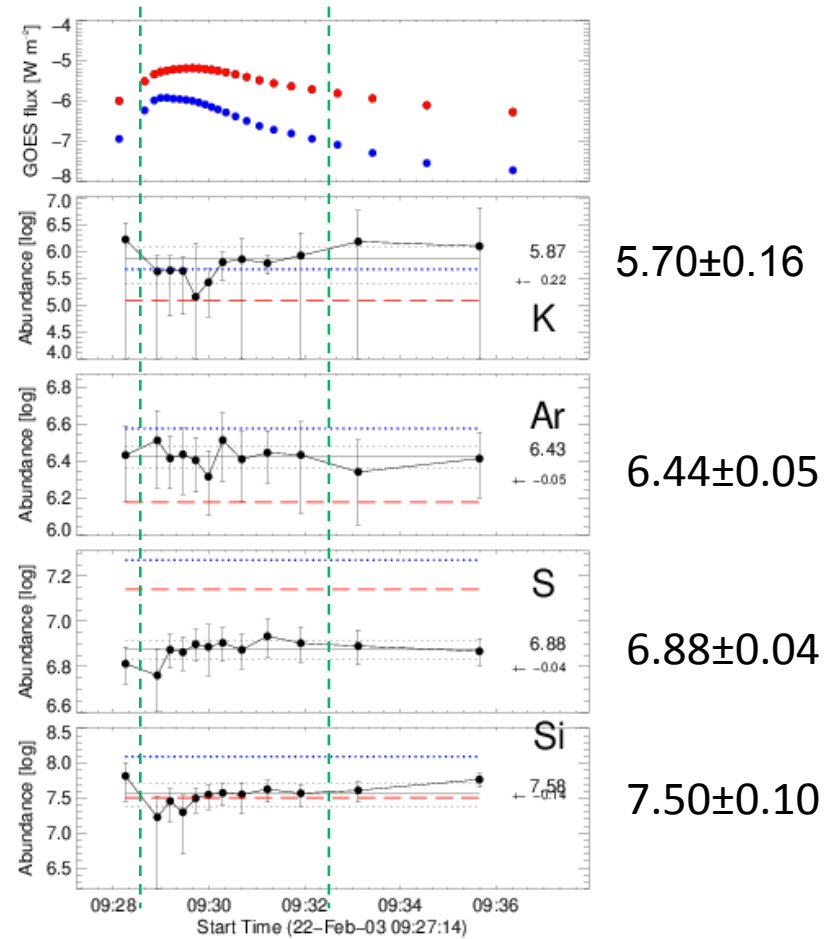
22 Feb. 2003 ~09:29 UT C 5.8

Results for individual flares
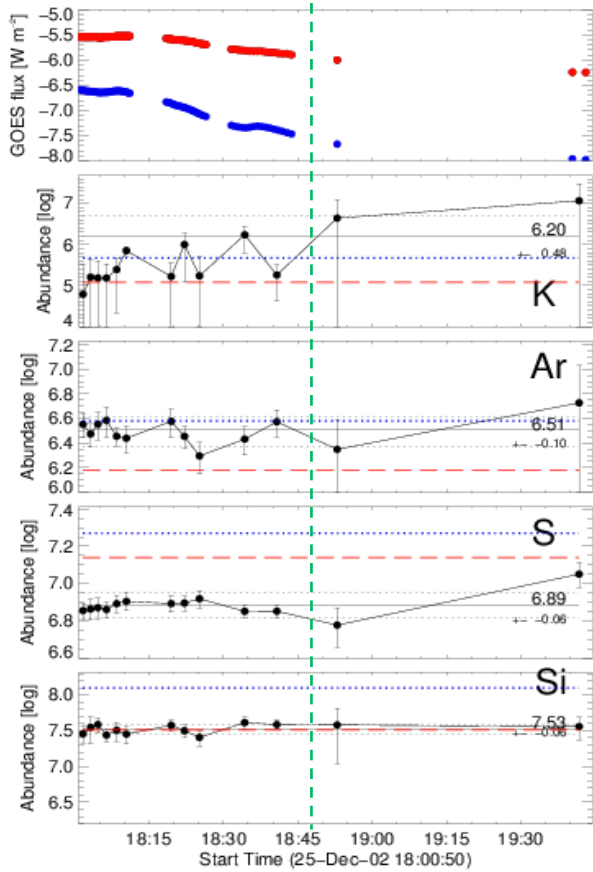
5.63±0.34

6.50±0.08

6.88±0.02

7.52±0.06
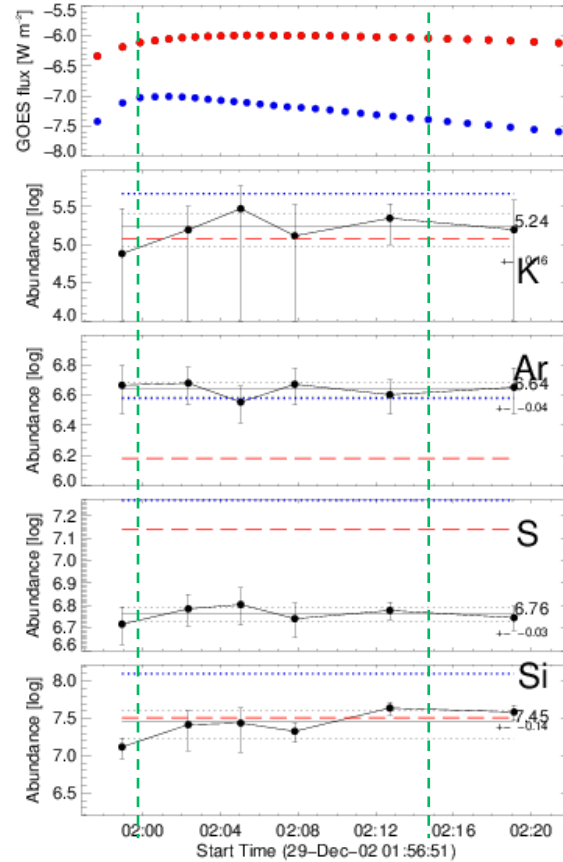
5.30±0.14

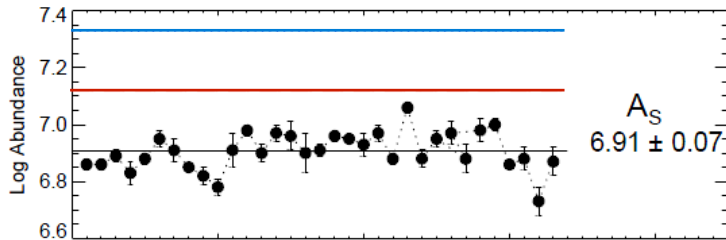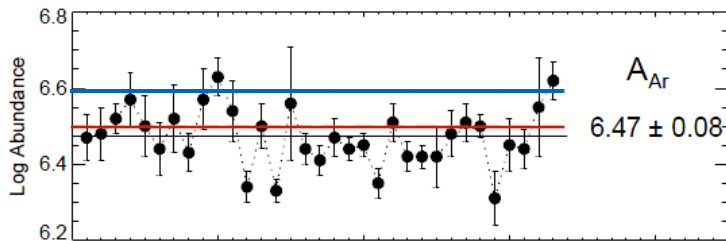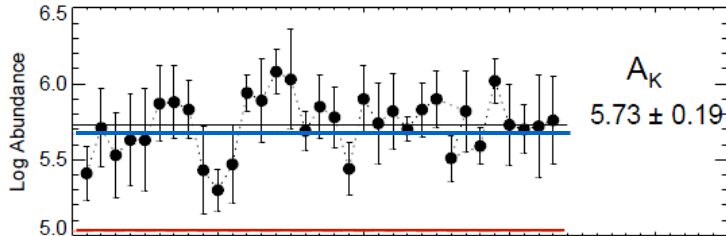6.63±0.05

6.78±0.03

7.47±0.12

25 Dec. 2002 ~ 18:09 UT C2.9

29 Dec. 2002 ~ 02:59 UT B9.9

Rather stabilized abundances during the flare evolution
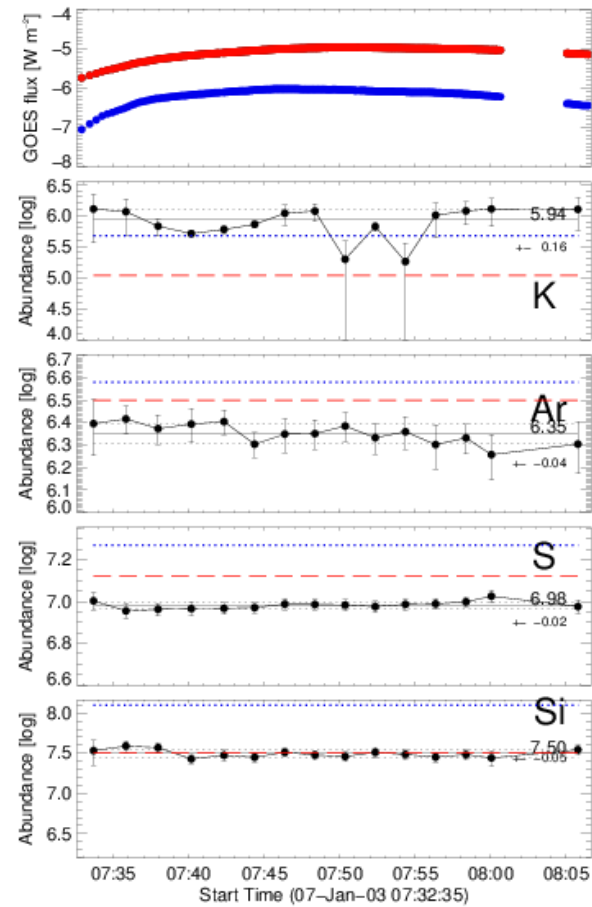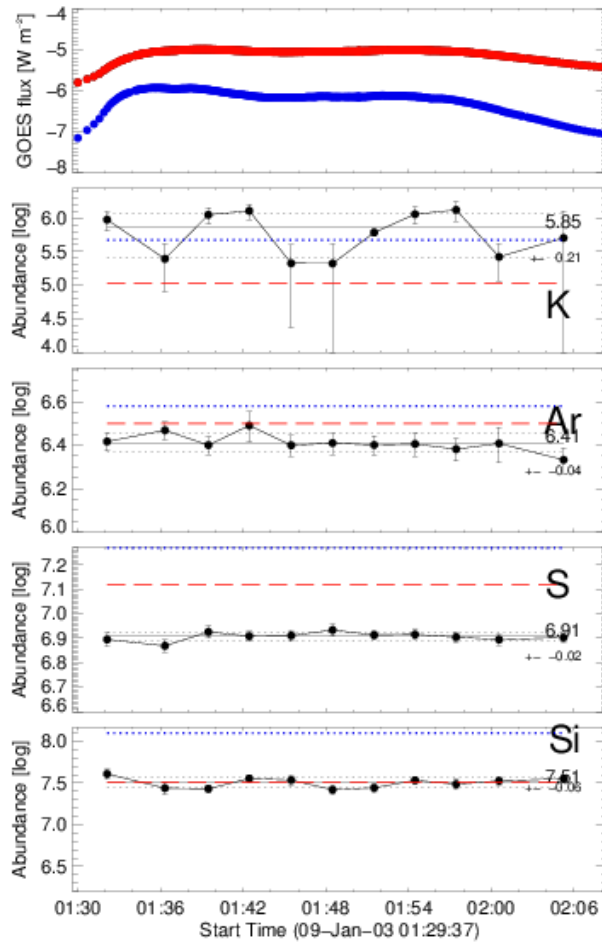
The main results
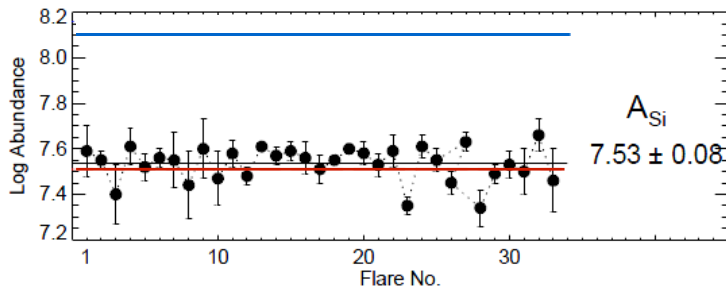
_____ Coronal abundances (Feldman et al., 1992; from CHIANTI database for K)

_____ Photospheric (Asplund et al., 2009; for Ar proxies from Lodders, 2008)

- K (FIP=4.34 eV) average abundance near coronal value (spread over a wide range from 5.3 to 6.1)
- Ar (FIP=15.76 eV) average abundance near photospheric but induvidual values are scuttered from 6.3 to 6.65
- S (FIP=10.36 eV) mean abundance **always below photospheric** (inverse FIP effect ??)
- Si (FIP=8.15 eV) abundance close to photospheric

Ar abundance

Phot_Grive	Meyer	Phot.	Cor_Feldm	Cor_ex	Cosmic
6.18	6.33	6.4	6.58	6.58	6.8

Concluding remarks

- The analysis of abundances for 33 flares observed with RESIK is made on non-isothermal assumption (multithermal approach)
- The present estimates (multithermal approach) of abundances for **Ar** and **K** are very close to that obtained previously (isothermal analysis). (*GOES* temp. well describes Ar XVII and K XVIII lines.) For **S** and **Si** values of obtained abundances are 1.8 and 2.1 times lower.
- There is only very little evidence of abundance variations with flare time evolution.
- Flare-to-flare variations seem to be ruled out for Si, S, and Ar but ±50% variations are not ruled out for K (but the larger uncertainty in its abundance estimate).
- The analysis has resulted in the following abundance estimates:

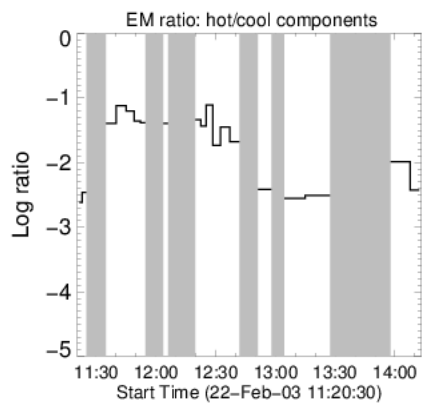|	
A(Ar) = 6.47 ± 0.08	(FIP=15.76 eV)
A(K) = 5.73 ± 0.19	(FIP=4.34 eV)
A(Si) = 7.53 ± 0.08	(FIP=8.15 eV)
A(S) = 6.91 ± 0.07	(FIP=10.36 eV)

22 Feb. 2003 flares

09:29 UT C 5.8 disc

12:20 UT C 1.7 limb

22 Feb. 2003 ~09:29 UT **C5.8** (disc)

T>9 MK

RESIK DEM evolution

EM ratio: hot/cool components

R=3.6"
2.6x10^8 cm
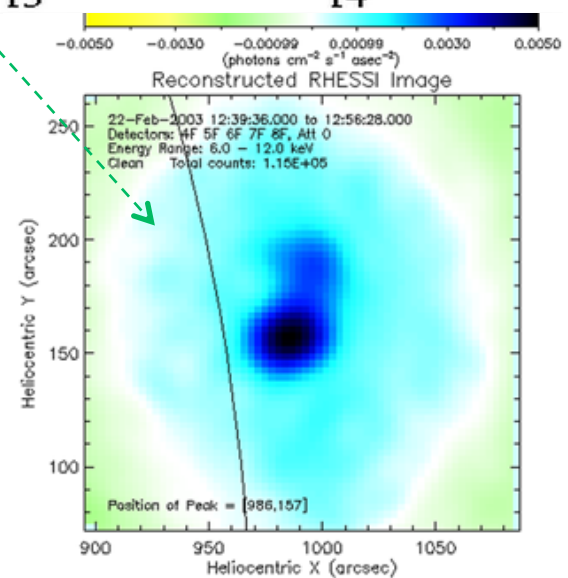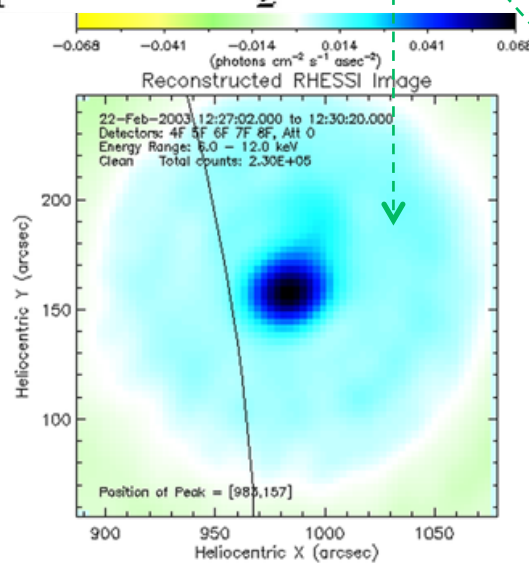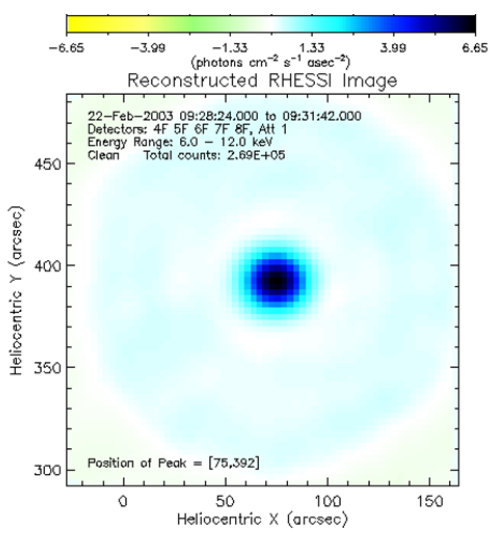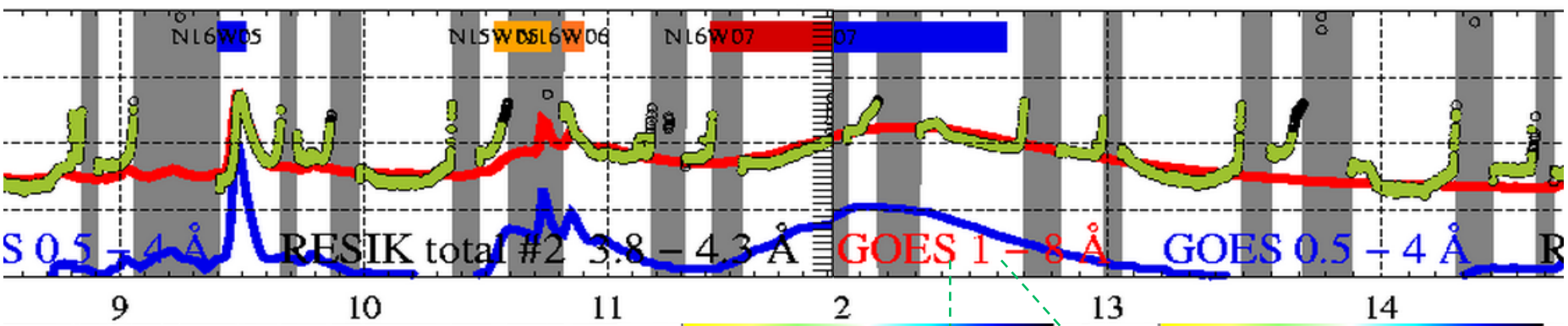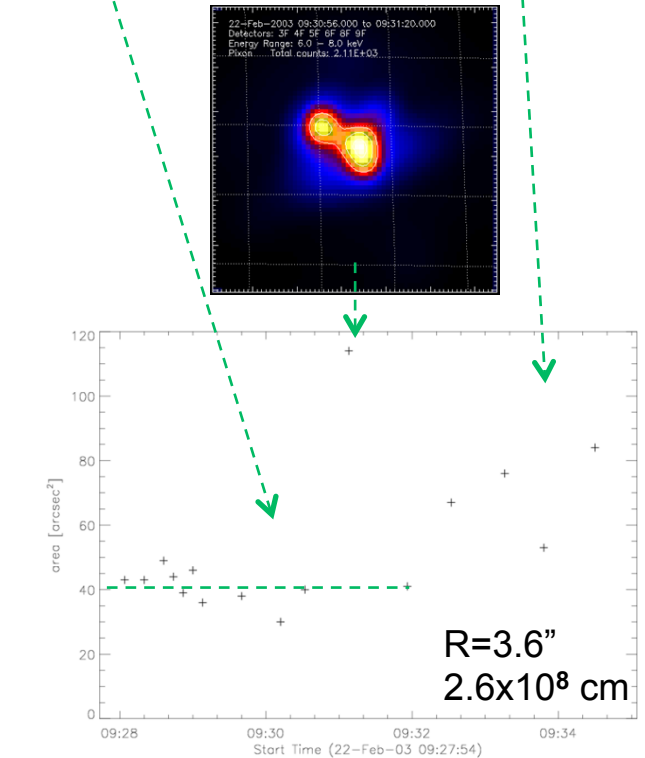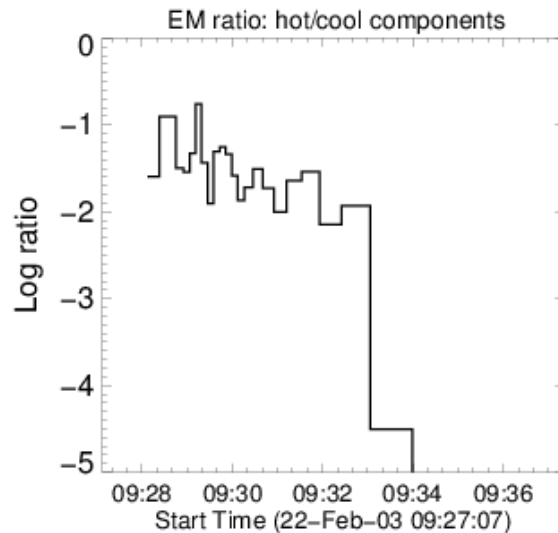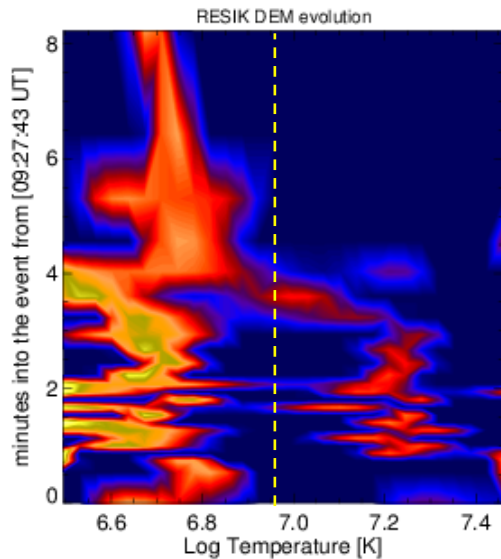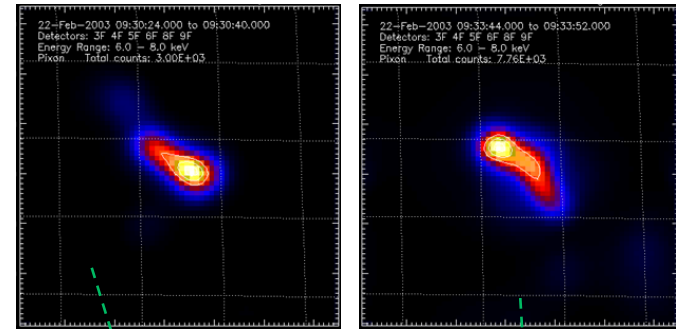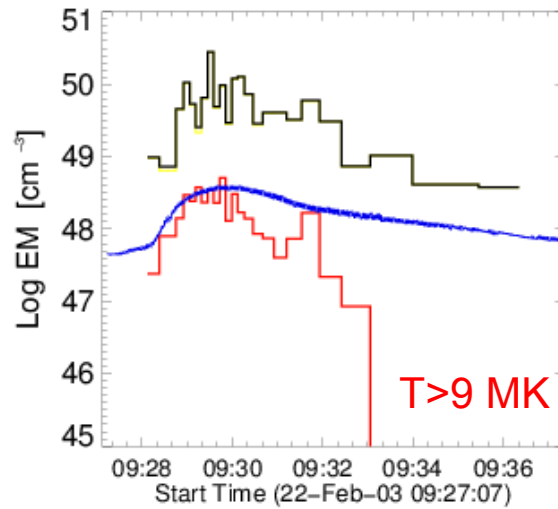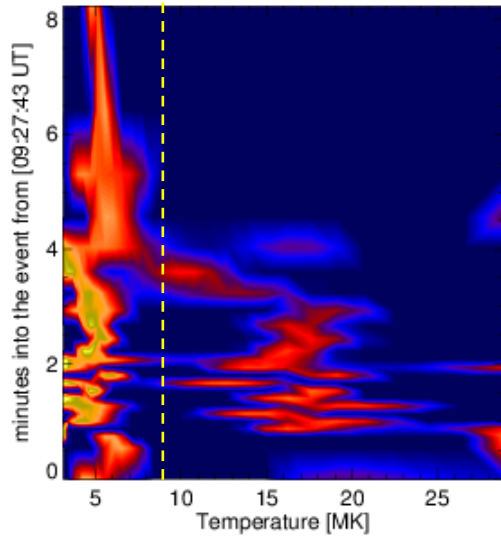
22 Feb. 2003 ~12:20 UT   **C1.7** (limb)
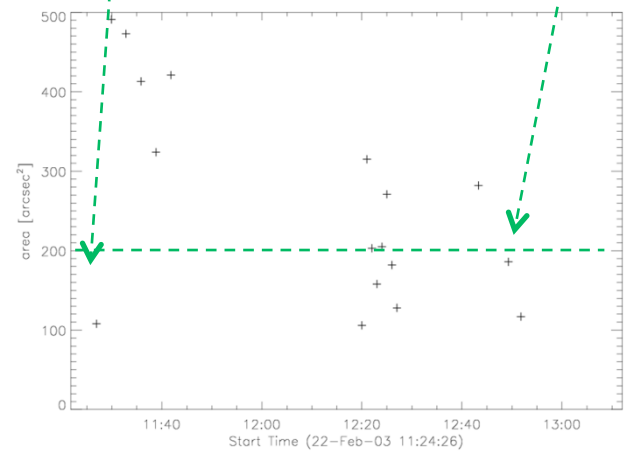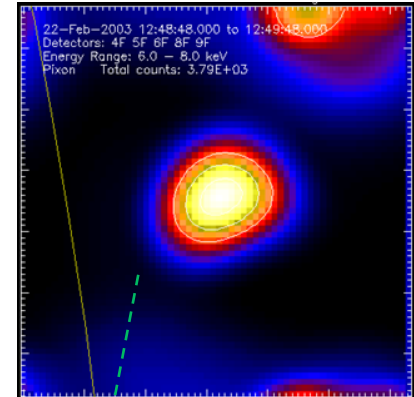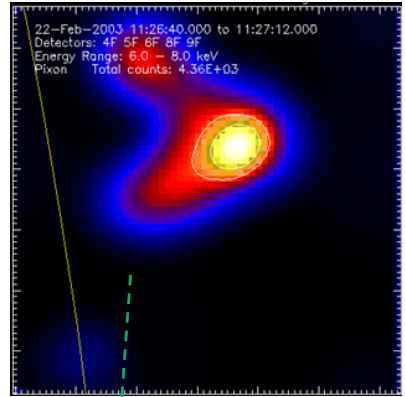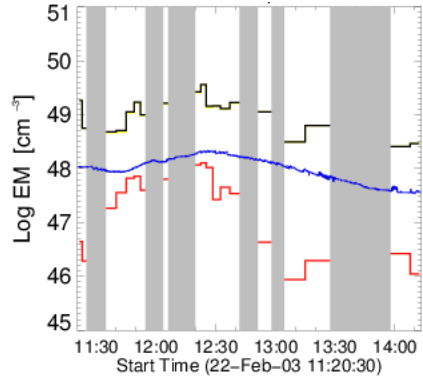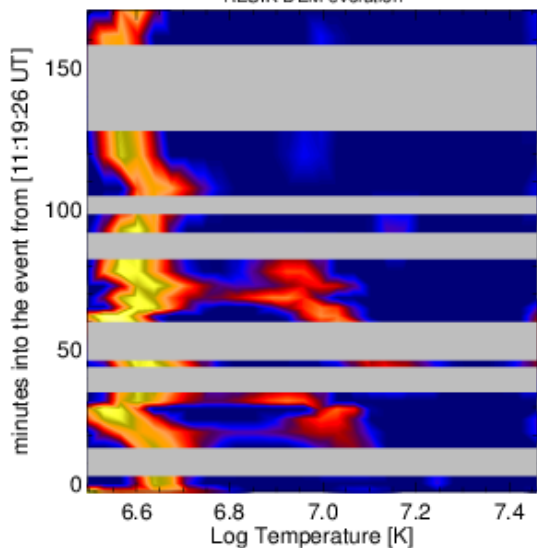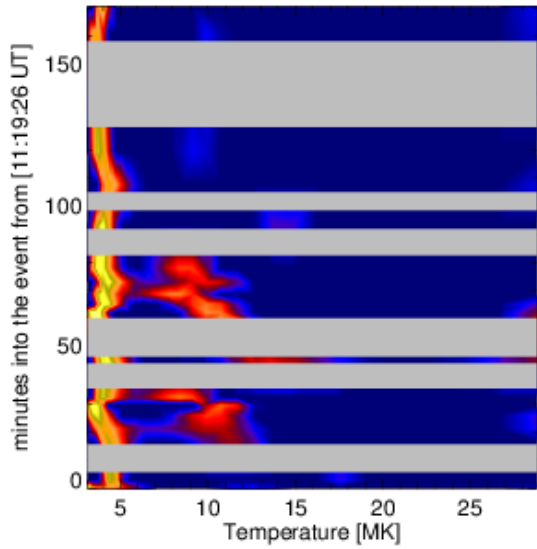
R=8"
5.8x10⁸ cm

Hot plasma's density determination

C 5.8 disc flare

C 1.7 limb flare

$N_e = 2 \times 10^{11}$ cm^{-3}

$N_e = 4 \times 10^{10}$ cm^{-3}